Comprehensive utilization of bauxite residue for simultaneous recovery of base metals and critical elements

Sustainable Materials and Technologies

Care Expiral, Linda Gaiter, Anthony No. (per Neglinal)

Himanshu Tanvar, Brajendra Mishra

PII: S2214-9937(22)00080-X

DOI: https://doi.org/10.1016/j.susmat.2022.e00466

Reference: SUSMAT 466

To appear in: Sustainable Materials and Technologies

Received date: 5 May 2022

Revised date: 24 June 2022

Accepted date: 1 July 2022

Please cite this article as: H. Tanvar and B. Mishra, Comprehensive utilization of bauxite residue for simultaneous recovery of base metals and critical elements, *Sustainable Materials and Technologies* (2022), https://doi.org/10.1016/j.susmat.2022.e00466

This is a PDF file of an article that has undergone enhancements after acceptance, such as the addition of a cover page and metadata, and formatting for readability, but it is not yet the definitive version of record. This version will undergo additional copyediting, typesetting and review before it is published in its final form, but we are providing this version to give early visibility of the article. Please note that, during the production process, errors may be discovered which could affect the content, and all legal disclaimers that apply to the journal pertain.

© 2022 Published by Elsevier B.V.

# Comprehensive utilization of bauxite residue for simultaneous recovery of base metals and critical elements

Himanshu Tanvar, Brajendra Mishra

Material Science and Engineering, Worcester Polytechnic Institute, Worcester, MA 01609, USA *Abstract* 

The growing stockpiles of bauxite residue and associated environmental hazards require a sophisticated recycling system for complete utilization and value recovery. The current application is limited as a raw material for building and construction applications. Considering the association of multiple elements (Fe, Al, Si, Ca, Ti, V, Se) within bauxite residue, metal extraction is of prime interest with respect to the economic value of the final product. The following study presents a hydrometallurgy-based process newsheet for the sustainable recovery of base metals and critical elements within bauxite residue. Major elements present in bauxite residue are recovered as materials for industrial ar plication, including high purity magnetite, alumina, titania, silica, and calcium carbonate. Trace elements are recovered in the liquid stream generated after the recovery of base metals.

#### 1. Introduction

Aluminum (Al) is the second most will by used metal globally and is primarily produced from bauxite ore. Despite the high recycling rate of scrap Al, more than 60 % is produced from bauxite through the Bayer and Hail-Héroult process (Habashi, 2016). The worldwide primary production of Al metal darmare 2021 was approx. 65.2 million tons, with 37.0 million tons alone from China (Bray, 2021). The global reserves of bauxite ore are estimated between 55 to 75 billion tons and are sufficient to meet the world demand well into the future (Bray, 2021). Production of alumina through the Bayer process results in producing a large quantity of caustic waste called bauxite residue or red mud. Approx. 1 – 1.5 tons of bauxite residue is generated per ton of alumina, and the annual waste generation is over 150 million tons, with a total of 3 – 4 billion tons accumulated by 2022 around the globe (Agrawal and Dhawan, 2021a; Anawati and Azimi, 2019; Evans, 2016).

Bauxite residue is characterized by fine particle size (80% passing 10 microns), high alkalinity (pH 10 - 12) and moisture (30 – 60 %) content (Khairul et al., 2019). The amount of moisture in

bauxite residue is determined by the solid-liquid separation process of individual Bayer refinery and impacts the storage conditions and requirements. The primary technology in Bayer refineries for solid-liquid separation is counter-current decantation which results in red mud slurry with more than 40 % solid content. Disposal, handling, and storage of such highly corrosive, low solid content slurry is expensive and requires a large land area (approx. 1 km<sup>2</sup> every 5 years for a 1 Mt/year alumina plant), generating potential health and environmental hazards (Ruyters et al., 2011; Tsakiridis et al., 2004). However, in recent years many Bayer refineries have adopted filter press technology to consolidate bauxite residue as high solid content residue (more than 70 % solid), resulting in dry storage (Healy, 2022). Dry storage has several advantages over traditional practice, including easy handling of residue, low land area required for storage and low maintenance cost of the storage facility. However, high a kal nity and salinity are the main chemical limitations to plant growth and rehabilitation of couxite residue storage lands, which leaves storage area un-vegetated and causes environmental problems (Di Carlo et al., 2020). Less than 4 % of the bauxite residue is utilized globally as an additive in the building and construction industries. The rest is stockpiled near the 'puzite processing plant and presents an alarming waste disposal situation (Evans, 2016). Baut te residue consists of mixed phases of iron (Fe, 5 – 60 %), Al (5-30 %), titanium (Ti, 1-15 %), calcium (Ca, 2-14 %), silicon (Si, 5-50 %), and sodium (Na, 1-15%) along with scar.drum (Sc, 0.001-0.012%), gallium (Ga, 0.001-0.011%) and vanadium (V, 0.03 - 0.2) %, as critical elements (Evans, 2016; Khairul et al., 2019; Ujaczki et al., 2018). Depencing on the geographic location of the alumina refinery, bauxite used, and processing parameter, the mineralogy of bauxite residue varies drastically (Borra et al., 2016a; Mishra and Costa, 2017; Swain et al., 2020). The presence of different elements including Fe, Ti, Al, Sc and V in the bauxite residue makes it a potentially lucrative source for metal extraction. Several research articles have been published investigating the extraction potential of valuable metals from bauxite residue; however, industrial-scale processing is still limited (Agrawal and Dhawan, 2021a; Ujaczki et al., 2018). The complex association of different elements, physical and chemical characteristics makes the extraction process expensive and challenging.

Basic metallurgical operations, including hydro and pyrometallurgical processes, are successful in recovering target elements from bauxite residue (Archambo and Kawatra, 2020a). Pyrometallurgical operations are mainly concerned with the recovery of Fe as pig iron or

magnetite concentrate (Borra et al., 2015a; Cardenia et al., 2018; Mishra et al., 2002). Smelting processes (Romelt process and EAF smelting) for recovery of metallic Fe are found successful on a pilot scale (Balomenos et al., 2012; Balomnenos et al., 2016). However, economic uncertainty due to high energy consumption is the limiting factor for industrial-scale applications (Anawati and Azimi, 2020; Archambo and Kawatra, 2020b). Furthermore, it results in the generation of poor-quality slag composed of Ca, Na, Al, Ti and Sc. There is very little information on slag processing for value recovery and is limited to the sulfation baking and leaching based route to dissolve Sc and Ti (Anawati and Azimi, 2020; Borra et al., 2015a).

Considering high selectivity, pure product, low capital and energy requirement, hydrometallurgical processes have been advancing progressively and adopted commercially in extractive metallurgy and recycling industries (Habashi, '005). The selection of reagents and processing conditions is critical in hydrometallurgic loperations to achieve high recovery. Hydrometallurgy-based studies are mainly concerned with the recovery of Sc and Ga from bauxite residue (Ding et al., 2022; Reid et al., 2017, Ujaczki et al., 2019). However, the low concentration of Sc, Ga and a high fraction of impurities (Fe, Al, Si, Ti, Na, Ca) demands high acid dosage during leaching and results in multi-element dissolution making downstream separation complicated and expensive (Ak il et al., 2017). These processes are concerned with the dissolution of elemental species, however, isolation and recovery of different elements from solution is limited (Agrawal and Dhawan, 2021b; Agrawal and Dhawan, 2021c; Borra et al., 2015b). Few literature works are concerned with recycling a high quantity of waste generated; therefore, scaleup efforts and industrial-scale processing are questionable for sustainable process development. Economically feasible, near-zero waste production hydrometallurgical flowsheet to recover both major (Fe, Al, Ca, Si, Ti) and minor (Sc, V) elements from bauxite residue is still lacking in the literature.

The following work presents a hydrometallurgical flowsheet using different lixiviants to selectively dissolve and recover metallic values at various stages of treatment. Hydrochloric acid (HCl), oxalic acid (H<sub>2</sub>C<sub>2</sub>O<sub>4</sub>), and sulfuric acid (H<sub>2</sub>SO<sub>4</sub>) are utilized as chemical reagents for dissolution of (Al, Si, Ca), (Fe, V), and (Ti, Sc), respectively. Whereas precipitation from solution, photochemical reduction and hydrolysis are adopted to recover the dissolved species selectively. Furthermore, an effort is made to utilize the waste solution generated during the

process. Solution recycling shows positive results in terms of regeneration of chemical lixiviant and additional value recovery for closed loop recycling process. A comprehensive flowsheet and material balance are presented to recover high purity magnetite, titania, alumina, calcium carbonate, and silica from bauxite residue. Focus is also made on the recovery of critical elements, including Sc and V in the proposed flowsheet. The present work is one of the few studies focused on recovering high purity magnetite, alumina and titania from bauxite residue using a hydrometallurgy-based process and results in simultaneous recovery of critical elements. Based on the experimental work, theoretical and economic analysis, the proposed process is economically feasible, results in near-zero waste discharge, and presents an excellent opportunity for industrial scale processing of bauxite residue.

#### 2. Experimental section

#### 2.1. Sample information and chemicals

The bauxite residue sample used in this study was are cured from an alumina refinery (Rio Tinto Alcan) located in Quebec City, Canada. The balk sample was collected from the dried section of the bauxite residue pond, dried in a laboratory oven at 110 °C for 12 h to remove residual moisture and further sieved below 250 n. icrons to remove large impurities (wood chips and pebbles). The bulk sample consistent of the (21.4 wt.%), Al (10.2 wt.%), Na (6.9 wt.%), Ca (2.3 wt.%), Si (5.0 wt.%), and Ti (3 wt.%). The concentration of trace metals of significant interest, including Sc and V, was 0.0016 % and 0.1074 %, respectively. The major phases determined from X-ray analysis consist of hematite (Fe<sub>2</sub>O<sub>3</sub>), boehmite (Al(OOH)), gibbsite (Al(OH)<sub>3</sub>), sodium aluminosilicate (1<sup>T</sup>a<sub>8</sub>Al<sub>6</sub>Si<sub>6</sub>O<sub>24</sub>(OH)<sub>2</sub>(H<sub>2</sub>O)<sub>2</sub>), calcium carbonate (CaCO<sub>3</sub>), quartz (SiO<sub>2</sub>), and anatase (TiO<sub>2</sub>).

#### 2.2. Experimental procedure

The simplified process flowsheet followed in this study is shown in Fig. 1. Bauxite residue was subjected to a multistage leaching and precipitation route for selective recovery of different metallic oxides at different stages of treatment.

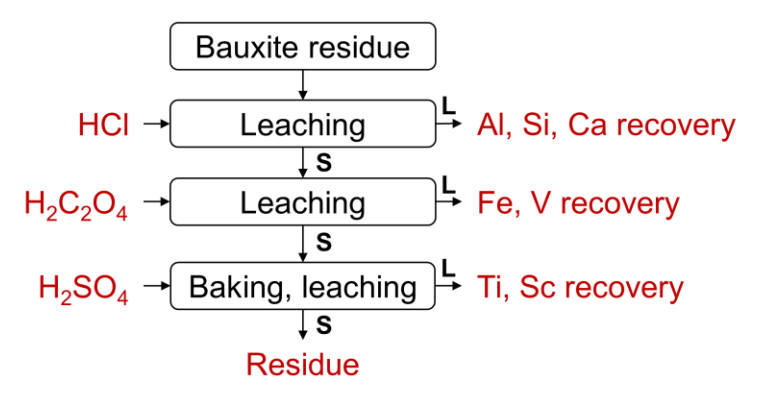


Fig. 1. Simplified processing flowsheet followed in this study.

#### 2.2.1. Bauxite residue neutralization

Bauxite residue was neutralized by leaching with 1 M HCl in 1000 mL Pyrex beaker at the following leaching conditions: 800 rpm stirring speed, 40° C temperature, 130 g/L pulp density, 15 min. time. The following operating condition was bas 'd on our previous work and resulted in maximum removal of alkali fraction while retaining other elements (Fe, Ti, Sc, V) in the residue (Tanvar and Mishra, 2021). The neutralized source was filtered to obtain neutralized bauxite residue and leach solution. The leach solution was subjected to polymerization and aging to recover dissolved Si and Al values. So tion aging was performed by adjusting the solution pH to 3 and keeping the solution ideal for 1 to 3 days to initiate polymerization. At the end of the aging period, polymerized silica vas filtered to obtain pH 3 precipitate and respective solution using vacuum filtration. The  $p_1$  of the solution was subsequently increased to 6.5 - 7 to precipitate aluminum hydroxide (pH 6 precipitate). Aluminum hydroxide precipitate was recovered after filtration and further calcined at 1000 °C for 1 h in a muffle furnace to obtain alumina (Al<sub>2</sub>O<sub>3</sub>). The solution after Al precipitation was subjected to carbonation to recover Ca precipitate. Carbonation experiments were carried out in a 2000 mL Erlenmeyer flask equipped with a gas dispenser. Pure CO<sub>2</sub> gas (> 98%) was passed through the solution at a flow rate of 200 mL per minute at atmospheric pressure for 30 min at pH 10. The carbonated slurry was filtered to obtain calcium carbonate precipitate and solution. Ammonium hydroxide solution was added to the solution under magnetic stirring to increase the pH of the solution to the desired value. All the solid products at different stages of precipitation were separated by vacuum filtration setup and dried in a laboratory oven at 98 °C for 24 h before characterization.

#### 2.2.2. Leaching with oxalic acid and photochemical reduction

Neutralized bauxite residue was leached with 2 M oxalic acid in a 1000 mL three-necked flat bottom Pyrex flask using a magnetic stirrer at the following conditions: 900 rpm stirring speed, 95 °C temperature, 100 g/L pulp density, 2.5 h time. One end of the flask was connected to a reflux condenser, while the other two ends were used to measure slurry temperature and add samples. The leached slurry was filtered using vacuum filtration setup to obtain ferric oxalate solution and residue.

The leach solution was subjected to ultraviolet (UV) light exposure for photochemical reduction of Fe (III) to Fe (II) and precipitation of ferrous oxalate. Precipit tion experiments were carried out in a Pyrex crystallization dish using a UV lamp of 100 W rower. UV lamp emitting UV A and B (280 – 400 nm) irradiations was fixed on the top to include the solution. UV exposure was performed for 6 h using 500 mL leach liquor under continuous stirring at 150 rpm. Optimized conditions for leaching with oxalic acid and photochemical reduction were selected based on our previous work (Tanvar and Mishra 2021). The ferrous oxalate precipitate was collected after filtration of reacted slurry and fundamental in a laboratory oven at 98°C for 24 h. The filtered solution obtained after precipitation was utilized for the next cycle of leaching with oxalic acid. The desired amount of oxalic acid was added to the solution to adjust the concentration at 2 M before leaching. The leach solution recycling was carried out nine times, and different residues, solutions and precipitates were collected and analyzed.

## 2.2.3. Ferrous oxalate decomposition

The ferrous oxalate prec pitate collected after photochemical reduction of ferric oxalate leach liquor was subjected thermal decomposition to produce magnetite. Decomposition experiments were performed in a tube furnace (MTI OTF-1200X) under an inert atmosphere to prevent oxidation of Fe(II) to Fe(III). Ferrous oxalate samples were heated to desired temperature (300 – 500 °C) with a heating rate of 9 °C/min, followed by decomposition for 1 h under a continuous flow of nitrogen gas (50 ml/min). The sample was cooled down to room temperature in a nitrogen atmosphere before taking out of the furnace to prevent oxidation.

#### 2.2.4. Sulfation baking and Ti hydrolysis

After leaching with oxalic acid, the resulting residue was subjected to sulfation baking using sulfuric acid to recover Ti and Sc. The solid samples were thoroughly mixed with the desired

amount of sulfuric acid (1.3 mL/g) to form a paste which was further transferred into a ceramic boat and heated in a tubular furnace at different temperatures (150 – 400 °C) for 2 h. The sulfated sample was pulverized using a mortar pestle and subsequently leached in 0.5 M sulfuric acid at 65 °C for 90 min. Leaching experiments were carried out 500 mL Pyrex beaker using a magnetic stirrer at 800 rpm stirring speed. The leach residue and leach liquor were separated using a vacuum filter, followed by thermal hydrolysis of leach liquor to recover Ti precipitate. Hydrolysis experiments were carried out by boiling the solution to 100 °C for 4 h in a 1000 mL Pyrex flask connected to a condenser.

#### 2.3. Analytical techniques

The chemical analysis of the samples was carried out using inductively Coupled Plasma – Optical Emission Spectroscopy and Mass Spectroscopy (TC) – OES (PerkinElmer Optima 8000), MS (PerkinElmer NEXION350x)). ICP-OES was used to analyze major elements, while ICP-MS for trace elements. Solid samples were fused virth borate flux at 1000 °C for 1 h, dissolved in 25 % nitric acid solution, diluted, and further analyzed with ICP – OES and MS. In contrast, the liquid samples were analyzed after dilution with 2 % nitric acid. Mineral phases present in the solid samples at different stages were determined using an X-ray diffractometer (XRD; PANalytical Empyrean). The diffract or cata were measured using a  $Cr - K_{\alpha}$  radiation in the 2 – theta range of 10 to 80°, with a scanning rate of 2 °/min and a step size of 0.02°. Thermodynamic information and standard Git's free energy of different reactions were determined using the Reaction module in FactSage 3 °C and HSC Chemistry 5.1 software.

#### 3. Results and discussion

#### 3.1. Bauxite residue neutralization and recovery of Al, Si, and Ca

Direct leaching of bauxite residue in acid solution requires an additional reagent because a part of it is consumed to neutralize the alkali left behind from the Bayer process. Neutralizing bauxite residue with HCl reduces the acid demand during the second stage of leaching with oxalic acid. Oxalic acid is relatively more expensive than HCl; therefore, neutralization with HCl reduces the overall reagent cost. Based on the preliminary oxalic leaching experiments, it was found that the oxalic acid consumption in the Fe leaching process is reduced by 32 % after neutralization of bauxite residue with HCl and product purity was enhanced significantly. Therefore, bauxite

residue was neutralized with HCl before leaching with oxalic acid. Carbonation of bauxite residue slurry is reported to reduce the pH to a neutral range (6-7) during continuous purging with CO<sub>2</sub>; however, the presence of unreacted sodalite and hydroxide buffers the pH of bauxite residue to an average value of 10 - 11 after CO<sub>2</sub> bubbling is stopped (Rivera et al., 2017). Carbonation is only efficient for removing freely available alkali and cannot dissociate the sodium aluminosilicate structure resulting in only 10-12 % Na removal. Therefore, leaching with mild HCl was adopted to neutralize and dissociate sodium aluminum silicate (sodalite, Na<sub>8</sub>Al<sub>6</sub>Si<sub>6</sub>O<sub>24</sub>(OH)<sub>2</sub>) phase and reduce the Na, Ca content below 1 %. The underlying chemical reactions of Na, Ca, Al, Fe, Si and Ti oxides with HCl, along with the respective Gibbs free energy at 40 °C, are shown in Eq. (1-6). A high negative value of Gibbs free energy for dissolution of Na, Ca, and Al shows a high thermodynamic tentency to attain equilibrium in a short duration of time. Whereas the less negative value of Cibbs free energy for Fe shows that the reaction is thermodynamically favorable, however is juires a high temperature and longer duration to reach equilibrium (Majima et al., 1985). Furthermore, positive values of Gibbs free energy for Ti and Si show that the reaction is not favored thermodynamically. The HCl leaching experiments were conducted for a short a ration (15 min) at 40 °C to dissolve the maximum fraction of alkali and retain Fe, Ti, Sc and V in the residue for subsequent recovery.

The chemical composition of bauring residue neutralized solid, and leach solution at optimized conditions (1 M HCl, 15 min, 4°°C, 130 g/L pulp density) based on our previous work is shown in Table 1 (Tanvar and Mishra, 2021). The HCl leaching resulted in the dissolution of 93.1 % Na, 92.7 % Ca, 59.3 % S, an 139.1 % Al. Whereas dissolution of Fe, Ti, Sc and V was less than 5 %. The pH of bauxite residue slurry dropped from 11 to 3 after neutralization. The XRD spectrum of neutralized residue presented in Fig. 2 (a) shows that the peaks corresponding to sodalite (2 theta = 20.8°, 52.39°) and calcite phase (2 theta = 44.4°) dissociated after HCl wash. The XRD analysis shows that HCl wash predominantly dissociated sodalite and calcium carbonate phases resulting in the dissolution of corresponding Na, Al, Si, and Ca values. The reaction of gibbsite and hematite with HCl is thermodynamically favored with negative value of Gibbs free energy; however, based on XRD analysis, both phases are evident in neutralized samples showing limited dissolution due to kinetic limitations. Since the HCl leaching was performed for 15 min, the sodalite and calcite phase reacted spontaneously, consuming most of

the free acid. In contrast, gibbsite and hematite did not react as sufficient time, temperature and acid were not provided for dissolution.

The solution obtained after HCl leaching (pH 2.7) mainly consists of 2882.82 ppm Ca, 8711.04 ppm Na, 3517.02 ppm Si, and 5309.20 ppm Al as dissolved species and was further processed for recovery of these elements. As per the standard E-pH diagram of the Al, Si, Na, Ca-O-H system, Al can be selectively precipitated as Al hydroxide in the neutral pH range (6-7). However, the dissolved silica forms a polymeric structure with monomers of Si(OH)<sub>4</sub> branched together to form polysilicic acid and caused a gelatinous solution. Direct increase of pH to 6 causes silica to polymerize and results in poor recovery and run v of Al product. Therefore, silica needs to be separated before Al recovery is attempted to chain a high purity product. The sol-gel method is widely applied to produce silica, cera ic and glass materials. The process involves dissolution of sodium silicate precursor in hineral acid (H2SO4, HCl) followed by hydrolysis and aging to produce silica gel which is further dried and calcined to produce aluminosilicate geopolymer (Hench and West 1520). The sol-gel method proceeds through a polymerization mechanism where the diss ilve i species of Si and Al form polymeric bonds of Si-O-Si and Si-O-Al and forms a long-chain polymeric gel in an acidic solution (Dimas et al., 2009; Giannopoulou and Panias, 2010). Silicit acid exists as isolated molecules in the form of monosilicic acid (Si(OH)<sub>4</sub>) and as linked molecules called polysilicic acid. As a function of time, polymerization degree reduces, and polymers decompose into short-chain species, which are stable and relatively easy to titer. The transformation of long-chain polymeric species to monomeric species and r specitive filtration ability is highly dependent on the pH of the solution, aging time, ionic strength, and other dissolved species (Dietzel, 2000).

Table 1. Chemical composition of bauxite residue, neutralized solid and HCl leach liquor.

Sampl	Quantit	Uni	Ca	Si	Ti	Na	Fe	Al	Sc	V
e	y	t								
Bauxit e residue	130 g	%	2.31	5.01	3.67	6.98	21.44	10.21	0.001 6	0.1
HCl residue	87.8 g	%	0.25	3.02	5.25	0.71	31.61	9.20	0.002	0.1 5

HC1	1000 mL	ppm	2882.8	3517.0	47.7	8711.0	197.2	5309.2	0.06	8.2
solutio			2	2	1	4	3	0		9
n										
Dissolu	Dissolution value (%)		92.68	59.25	1.30	93.12	0.33	39.09	4.59	3.5
										1

$$NaOH + HCl \rightarrow NaCl + H_2O \ (\Delta G_{40^{\circ}C}^{\circ} = -121.31 \ kJ/mol) \ (1)$$
 $CaCO_3 + 2HCl \rightarrow CaCl_2 + H_2O + CO_2 \ (\Delta G_{40^{\circ}C}^{\circ} = -63.47 \ kJ/mol) \ (2)$ 
 $Al(OH)_3 + 3HCl \rightarrow AlCl_3 + 3H_2O \ (\Delta G_{40^{\circ}C}^{\circ} = -59.56 \ kJ/mol) \ (3)$ 
 $Fe_2O_3 + 6HCl \rightarrow 2FeCl_3 + 3H_2O \ (\Delta G_{40^{\circ}C}^{\circ} = -0.65 \ kJ/mol) \ (4)$ 
 $SiO_2 + 2H_2O \rightarrow H_4SiO_4 \ (\Delta G_{40^{\circ}C}^{\circ} = 261.51 \ kJ/mol) \ (5)$ 
 $TiO_2 + 4HCl \rightarrow TiCl_4 + 2H_2O \ (\Delta G_{40^{\circ}C}^{\circ} = 82.49 \ kJ/mol) \ (6)$ 

The silica gelation method was applied to the HCl leach Equor to precipitate and separate silica, followed by recovery of Al and Ca. The pH of the solution was adjusted to approx. 3 followed by aging for polymerization of silica. It was observed that after aging for 1 day the concentration of Si in Al precipitate was 2.02 % and decreased to 0.06 % after 3 days. The pH 6 precipitate obtained from 3-day aged solution yielded Al precipitate with minor impurities (< 0.5 %) of Ca, Si and Na. The pH 3 precipitate is mainly composed of Si (25 – 30 %) along with Na (~ 2.5 %) and Al (7 – 9 %). Association of Al in the Si-O-Al polymeric chain results in coprecipitation and loss of Al values. More than 29 % Si was precipitated at pH 3 condition along with 21.4 % of dissolved Al. Furthermore Al was completely precipitated at pH 6 while retaining Ca and Na in the solution. The XRD spectrum and chemical analysis of pH 3 (silica) and calcined pH 6 precipitate are shown in Fig. 2 (b). pH 3 precipitate shows a characteristic broad peak of amorphous silica at a 2-theta value of approx. 25°, whereas calcined pH 6 precipitate shows peaks corresponding to alumina (Al<sub>2</sub>O<sub>3</sub>).

The solution obtained after Si and Al separation consist of approx. 2799.09 ppm Ca and 8634.11 ppm Na as the major elements. Recovery of Ca was attempted through three routes: precipitation as sulfate, hydroxide, and carbonate. The chemical reaction and respective Gibbs free energy for the reactions are shown in Eq. (7-9). The addition of sulfuric acid to the solution resulted in the precipitation of calcium sulfate, while the addition of NaOH generated calcium hydroxide precipitate. Precipitation in the form of carbonate using CO<sub>2</sub> gas was found efficient, with a high

thermodynamic tendency and faster reaction rate at moderate pH conditions. The CO<sub>2</sub> gas reacts with water to form carbonic acid (H<sub>2</sub>CO<sub>3</sub>), further dissociating to H<sub>2</sub>CO<sub>3</sub>/HCO<sub>3</sub><sup>-</sup> and HCO<sub>3</sub><sup>-</sup>/CO<sub>3</sub><sup>2-</sup> at pKa<sub>1</sub> = 6.35, pKa<sub>2</sub> = 10.2 respectively at 25°C (Marin Rivera and Van Gerven, 2020). The carbonate and bicarbonate ions react with dissolved species to form carbonate salts. Furthermore, the carbonation process has an additional advantage of carbon sequestration and will help reduce greenhouse gas emissions with a carbonation capacity of 17 kg CO<sub>2</sub> per ton of bauxite residue. The XRD spectrum of Ca precipitate obtained after sulfation, carbonation, and hydroxyl precipitation shows the presence of calcium sulfate, carbonate, and hydroxide, respectively, as shown in Fig. 2 (c). Almost all the Ca was recovered as calcium carbonate after 30 min carbonation, and the filtered solution consists of Na (85.0.1 ppm) as the only dissolved species in the form of chloride. The solution pH was approx 7 and can be processed through a desalination unit to separate NaCl and reuse water for acid neutralization. The leaching of bauxite residue with mild HCl provides the dual advantage of neutralization and recovery of value-added side products, including aluminosilitate geopolymer, ceramic grade alumina, and high purity calcium carbonate.

$$CaCl_{2} + CO_{2} + NaOH \rightarrow CaCO_{3} \downarrow + 2N \downarrow Cl + H_{2}O \ (\Delta G_{25^{\circ}C}^{\circ} = -100.59 \ kJ/mol) \ (7)$$

$$CaCl_{2} + 2NaOH \rightarrow Ca(O_{1}) \downarrow + 2NaCl \ (\Delta G_{25^{\circ}C}^{\circ} = -27.29 \ kJ/mol) \ (8)$$

$$CaCl_{2} + H_{2}SO_{4} \rightarrow CaSC_{4} \downarrow + 2HCl + H_{2}O \ (\Delta G_{25^{\circ}C}^{\circ} = -70.73 \ kJ/mol) \ (9)$$

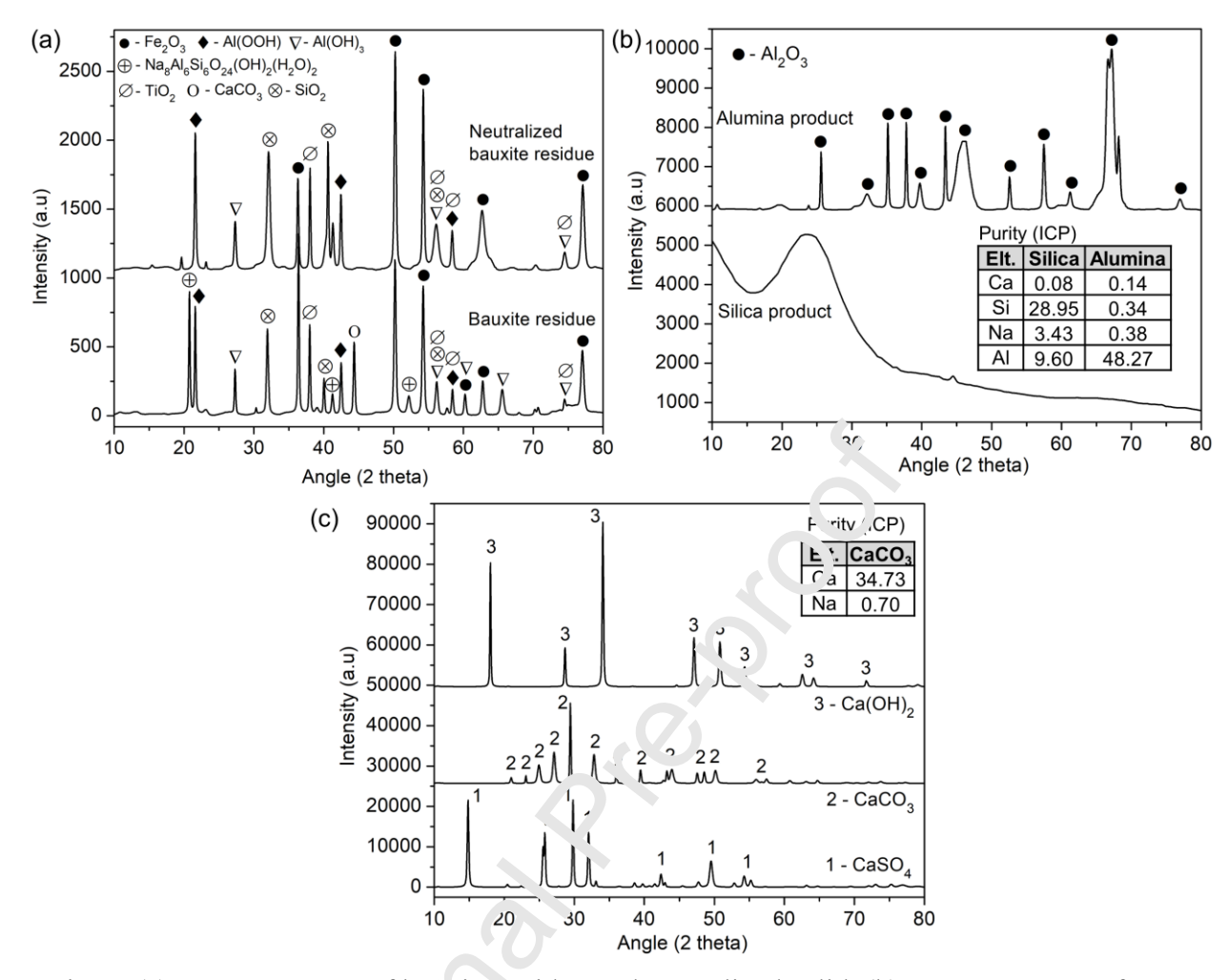


Fig. 2. (a) XRD spectrum of bau rite residue and neutralized solid, (b) XRD spectrum of pH 3 (silica) and calcined pH 6 precipitate, (c) XRD spectrum of different Ca precipitate.

#### 3.2. Fe leaching and pre ipin tion

The neutralized bauxite residue was further leached with oxalic acid to dissolve Fe as ferric oxalate, followed by photochemical reduction of leach liquor to precipitate ferrous oxalate and subsequent decomposition to magnetite. Oxalic acid is an organic acid with a high affinity towards Fe and V due to its chelating ability and stability (Taxiarchou et al., 1997). Oxalic acid dissociated into  $HC_2O_4^-$  and  $C_2O_4^{2-}$  at pH < 4 and pH > 4, respectively, and forms a coordination bond with metal ions (such as  $Fe^{3+}$ ,  $V^{5+}$ ), resulting in dissolution. The Fe leaching mechanism follows both reductive and non-reductive reaction pathways at different operating conditions, as per the chemical reactions shown in Eq. (10) – (12). The non-reductive reaction pathway involves adsorption of oxalate ion onto the solid particle and desorption of surface ferric ion

complex into the solution and possesses high activation energy. Non-reductive dissolution results in the formation of  $[Fe(C_2O_4)_3]^{3-}$  (Eq (10)) and  $[FeHC_2O_4]^{2+}$  (Eq. (11)) at high (> 4) and low pH (< 2), respectively. On the other hand, reductive dissolution is favored at lower temperatures and results in the formation of  $[Fe(C_2O_4)_2]^{2-}$  complex (Eq. (12)). The reductive mechanism involves generation of ferrous ions via electron transfer from adsorbed complex to surface ferric ion and is a slow process. Based on our previous work and literature findings, the activation energy for dissolution of hematite using oxalic acid was determined as 100 – 150 kJ/mol in the temperature range of 65 to 95 °C following a non-reductive dissolution mechanism (Lee et al., 2006; Salmimies et al., 2012; Tanvar and Mishra, 2021). Both reductive and non-reductive pathways are thermodynamically favored at 25 °C; however, the slower knetics requires a longer leaching duration; therefore, high-temperature dissolution is preferred to accelerate the kinetics. Furthermore, non-reductive dissolution can be advantageous over reductive dissolution, considering the stability of leach liquor. In reductive dissolution, Fe (II) oxalate can be precipitated from the solution as hydrated ferr vs oxalate (FeC<sub>2</sub>O<sub>4</sub>.2H<sub>2</sub>O) during leaching, solution, which can be further reduced to propitate ferrous oxalate for clean separation.

On the other hand,  $V_2O_5$  reacts with d.s. Of ed oxalic acid species ( $HC_2O_4^-$  and  $C_2O_4^{-2}$ ) through a reductive reaction mechanism to  $f_{C_1, T_1}$  collable  $VO^{2+}$  complex in the solution as per Eq. (13) and (14). The V species in the lear h solution exists as  $VO(C_2O_4)_2^{2-}$  with a stable  $\pi$ - $\pi$  conjugated system between the O-C-O bond of  $C_2O_4^{2-}$  and V=O bond of  $VO^{2+}$  (Hu and Zhang, 2021; Li et al., 2021). Photochemical realiction using UV light was performed to reduce ferric oxalate in the leach solution to ferrors oxalate while retaining V(IV) in the solution. Ferric oxalate ([Fe( $C_2O_4$ )<sub>3</sub>]<sup>3-</sup>) is a photochemically active complex and induces a ligand to metal charge transfer under UV irradiation resulting in the formation of [Fe( $C_2O_4$ )<sub>2</sub>]<sup>2-</sup>,  $CO_2$  and  $C_2O_4^{2-}$  ions in the solution as per Eq. (15). [Fe( $C_2O_4$ )<sub>2</sub>]<sup>2-</sup> is further hydrolyzed in the solution according to the reaction shown in Eq. (16) and results in the precipitation of ferrous oxalate dihydrate (Fe $C_2O_4$ .2H<sub>2</sub>O). On the other hand, the thermodynamically stable V(IV) oxalate species in the solution remains dissolved and does not precipitate with Fe(II) oxalate. During the photochemical reduction process, electron transfer from ligand (oxalate) to metal (Fe<sup>3+</sup>) generates a  $C_2O_4^+$  free radical anion in the solution, which is extremely unstable and undergoes spontaneous dissociation into  $CO_2$  and  $CO_2^+$ . The  $CO_2^+$  anion can further reduce another Fe<sup>3+</sup>

ion or combine with another  $CO_2^{\bullet}$  anion to form  $C_2O_4^{2^{\bullet}}$  ion in the solution (Mangiante et al., 2017). Reduced ferrous ion is precipitated, while oxalate ion regenerated remains dissolved.

$$\begin{split} Fe_2O_{3(s)} + 6C_2O_{4(aq)}^{2-} + 6H_{(aq)}^+ &\to 2[Fe(C_2O_4)_3]_{(aq)}^{3-} + 3H_2O_{(l)} \ (\Delta G_{25^{\circ}C}^{\circ} = -212.75 \ kJ/mol) \ (10) \\ Fe_2O_{3(s)} + 2HC_2O_{4(aq)}^- + 6H_{(aq)}^+ &\to 2[FeHC_2O_4]_{(aq)}^{2+} + 3H_2O_{(l)} \ (\Delta G_{25^{\circ}C}^{\circ} = -87.35 \ kJ/mol) \ (11) \\ Fe_2O_{3(s)} + 5C_2O_{4(aq)}^{2-} + 6H_{(aq)}^+ &\to 2[Fe(C_2O_4)_2]_{(aq)}^{2-} + 3H_2O_{(l)} + 2CO_{2(g)} \ (\Delta G_{25^{\circ}C}^{\circ} = -152.29 \ kJ/mol) \ (12) \\ V_2O_{5(s)} + 5HC_2O_{4(aq)}^- + H_{(aq)}^+ &\to 2[VO(C_2O_4)_2]_{(aq)}^{2-} + 3H_2O_{(l)} + 2CO_{2(g)} \ (\Delta G_{25^{\circ}C}^{\circ} = -326.05 \ kJ/mol) \ (13) \\ V_2O_{5(s)} + 5C_2O_{4(aq)}^{2-} + 6H_{(aq)}^+ &\to 2[VO(C_2O_4)_2]_{(aq)}^{2-} + 3H_1O_{(l)} + 2CO_{2(g)} \ (\Delta G_{25^{\circ}C}^{\circ} = -448.05 \ kJ/mol) \ (14) \\ [Fe(C_2O_4)_3]^{3-} &\to 2[Fe(C_2O_4)_2]^{2-} + 2C_2O_4^{2-} \ (15) \\ [Fe(C_2O_4)_2]^{2-} + 2H_2O_{0}^+ FeC_2O_4.2H_2 \\ &\to C_2O_4^{2-} \ (16) \end{split}$$

The leaching experiments were conducted using 2  $\times$ 1 oxalic acid solution at 95 °C for 2.5 h and 100 g/L pulp density. The photochemical reduction was performed for 6 h using a 100 W UV lamp. Leaching resulted in the dissolution of approximately 82.4 % Fe, 77.9 % V, 16.9 % Sc, 4.2 % Ti, 12.7 % Si, and 48.5 % Al. Furthermore, after photochemical reduction, more than 99 % of the Fe in the solution was recover as ferrous oxalate precipitate. In our previous work, leaching with oxalic acid and photochemical reduction process was optimized and thoroughly investigated to recover ferrous oxalate from bauxite residue (Tanvar and Mishra, 2021). The present work focuses on the regeneration of oxalic acid in the leaching circuit with the utilization of waste liquor generated after Fe precipitation. Regeneration of oxalic acid and utilization of waste solution will bolster the recycling process with reduced acid consumption and minimal waste generation. The solution after Fe precipitation was further recycled for the subsequent leaching to utilize the regenerated oxalate ion during reduction. It was found that after one cycle of solution recycling, the leaching of Fe was enhanced from 82.4 % to 90.6 % under the same conditions, while the dissolution of other elements remained the same (approx. 50.3 % Al, 4.7 % Ti, 7.4 % Si).

The dissolution value and extraction yield (precipitation efficiency) at different leaching – precipitation cycles are shown in Fig. 3 (a) and (b). During the solution recirculation

experiments, oxalic acid was found to crystallize out of the reduced solution, depicting that the solution contains an excess of oxalic acid beyond its solubility limit at room temperature (90 g/L). Therefore, after four cycles, no oxalic acid was added to utilize the excess oxalic acid in the solution. It is important to mention that no fresh oxalic acid was added to leaching during cycle number 5 and 9; therefore, the dissolution values obtained are due to regenerated oxalic acid in the solution. Results indicate that approx. 56.3 % of Fe was leached at the fifth cycle and 76.1 % at the ninth cycle without adding any oxalic acid.

The chemical analysis of solution after photochemical reduction at different leaching – precipitation cycles is shown in Fig. 3 (c). The precipitation efficiency of Fe decreased from 99.1 % to 95.7 % after the fifth cycle, and Fe concentration in the solution increased from 220.3 ppm in the first cycle to 1266.1 ppm in the ninth cycle. The increase in the concentration of other ions (mainly Al) in the solution limits the photochemical reduction capacity of Fe. However, the decrease in extraction ratio is very low (< 4 %) and does not affect the recovery process to a greater extent providing consistent product purity with reduced acid demand. The Al leaching was found consistent throughout the leaching sycies with approx. 45 - 50 % Al dissolution and was collectively recovered in the solution atter ferrous oxalate precipitation. The concentration of Al was increased from 3595.5 ppm diving the first cycle to approx. 15113.2 ppm at the end of the ninth cycle. The dissolved Al an be further recovered through pH adjustment and an ion exchange process for additional alumina recovery. The concentration of V increased from 58.4 ppm during the first cycle to 1.79.1 ppm during the second cycle and further saturated in the solution at approx. 141.8 pp 1 after the fourth cycle. The solution after nine cycles consists of 659.0 ppm Ca, 108.1 ppn Si, 1579.4 ppm Ti, 332.5 ppm Na, 1266.1 ppm Fe, 173.4 ppm V and 15113.2 ppm Al.

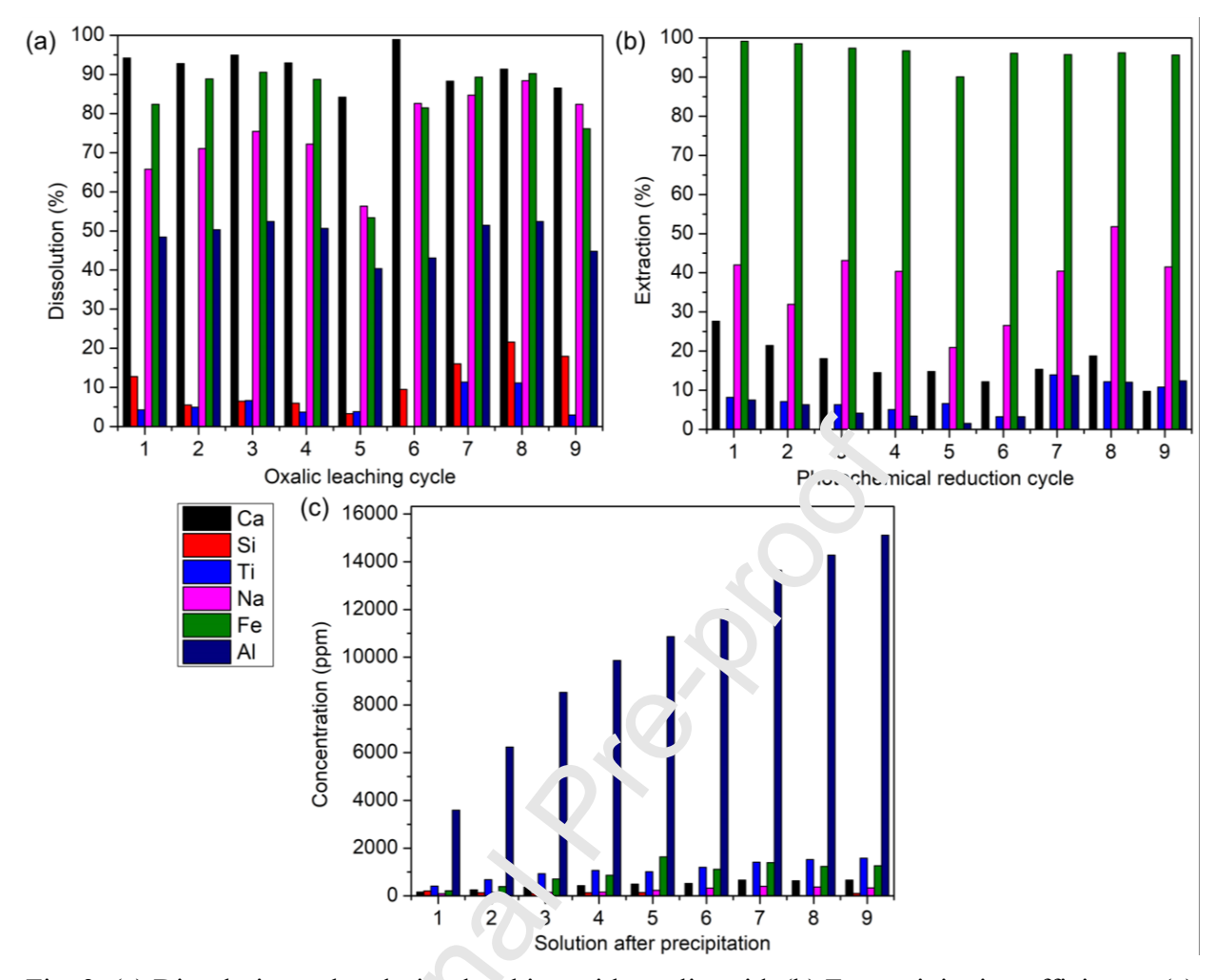


Fig. 3. (a) Dissolution value during leaching with oxalic acid, (b) Fe precipitation efficiency, (c) Sourtion concentration after precipitation.

The chemical composition and XRD spectra of oxalic acid leaching residue and ferrous oxalate precipitate at different lea hing – precipitation cycles are shown in Fig. 4 (a - d). The residue at different cycles consists of approx. 11 – 14 % Ti, 10 – 12 % Al, 4 – 6 % Si and 8 – 10 % Fe as major elements. XRD spectra show the presence of boehmite, anatase and rutile as the major phases. Peaks corresponding to hematite and gibbsite were not identified in the residue, reflecting complete dissociation during leaching. The chemical analysis of ferrous oxalate precipitate indicates consistent purity throughout the solution recycling experiments with less than 1 % of Na, Ca, and Al impurities. The XRD spectrum of precipitate confirms the presence of orthorhombic crystals of ferrous oxalate.

The photochemical reduction was found successful in selective recovery of high purity ferrous oxalate and regenerating oxalic acid in the process further utilized with solution reuse. Based on the calculations, oxalic acid demand was decreased up to 30 % during each cycle of solution recycling and is significant. Consistent product purity and residue composition throughout the nine cycles presents a great potential to reuse solution providing reduced acid demand, minimal waste generation and a high recovery rate. Furthermore, the isolation and recovery of Ti in the residue and V in the solution after Fe precipitation presents future scope for the recovery of these critical elements.

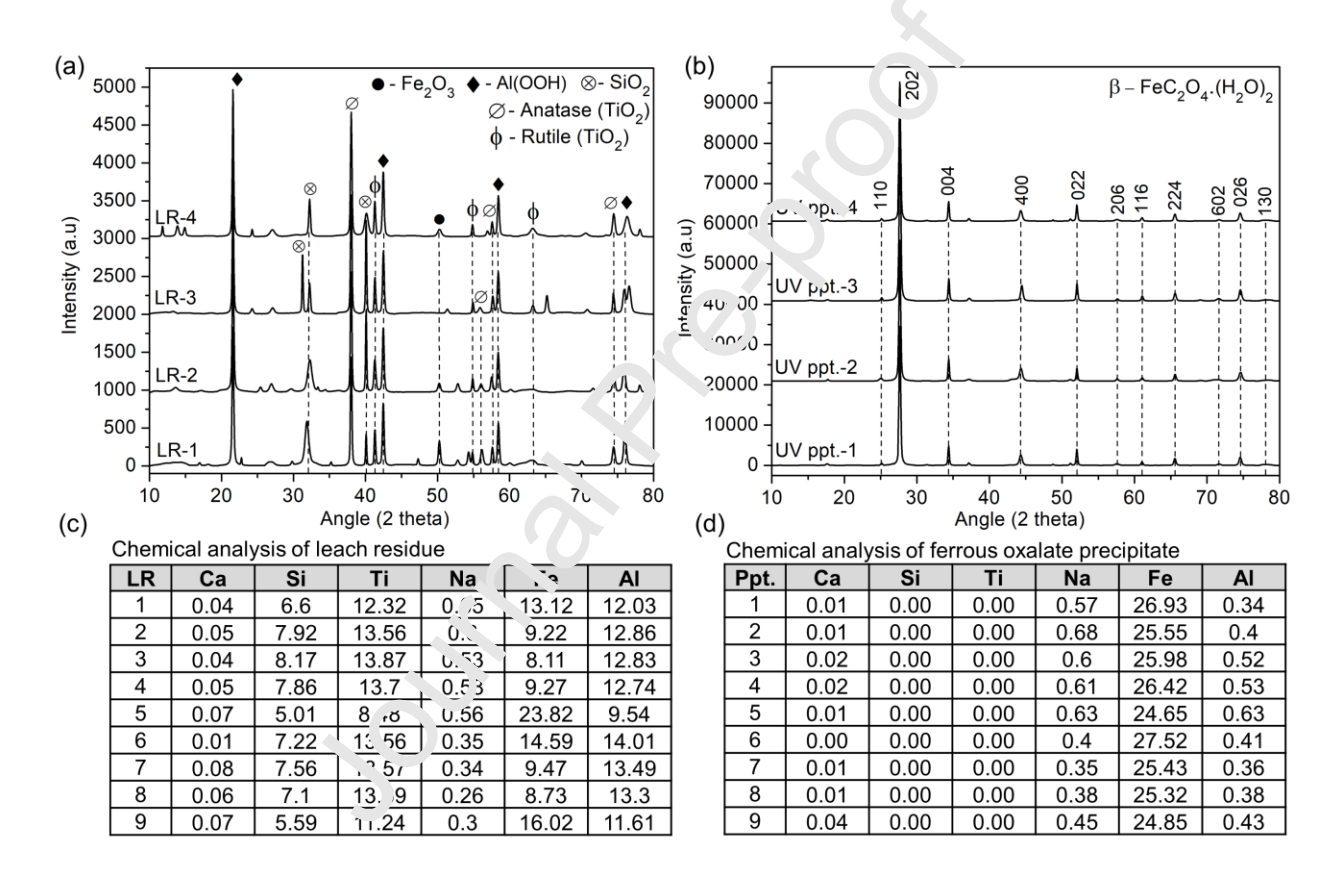


Fig. 4. XRD spectrum of (a) leaching residue and (b) ferrous oxalate precipitate, Chemical analysis of (a) leaching residue and (b) ferrous oxalate obtained at different solution recycling experiments.

#### 3.3. Ferrous oxalate to magnetite decomposition

The ferrous oxalate obtained after photochemical reduction was decomposed in an inert atmosphere to produce magnetite. A low oxygen atmosphere was maintained using a continuous

flow of N<sub>2</sub> in the tube furnace to restrict the oxidation of Fe<sup>+2</sup> to Fe<sup>+3</sup>. The thermogravimetric analysis of ferrous oxalate precipitate in the temperature range of 25 – 600 °C under 8 °C /min heating rate and nitrogen atmosphere is shown in Fig. 5. Dehydration and loss of water of crystallization from FeC<sub>2</sub>O<sub>4</sub>.2H<sub>2</sub>O results in the formation of FeC<sub>2</sub>O<sub>4</sub> up to a temperature of 230 °C. FeC<sub>2</sub>O<sub>4</sub> further dissociates into Fe<sub>3</sub>O<sub>4</sub> above 230 °C temperature together with gaseous CO and CO<sub>2</sub>. Crystallization of magnetite is accompanied by the decomposition of FeC<sub>2</sub>O<sub>4</sub> to iron carbide (Fe<sub>3</sub>C) with CO gas above 360 °C. Iron carbide dissociates into Fe and C in the 415 – 535 °C temperature range. In the final stage of reaction, magnetite is reduced to wüstite (FeO) in the presence of CO above 535 °C (Hermanek et al., 2006). Therefore, the decomposition atmosphere is critical for producing desired phases after thermal decomposition. A series of experiments were conducted in the temperature range of 300 – 500 °C for 1 h to identify optimal decomposition conditions. XRD spectrum of decomposition, product at different conditions is shown in Fig. 6 (a). The XRD of the sample heated at 300 °C shows the dehydrated ferrous oxalate (FeC<sub>2</sub>O<sub>4</sub>) phase. Maghemite (γ-Fe<sub>2</sub>O<sub>3</sub>) phase was detected in the 400 °C sample, while magnetite was the primary phase found above 430 °C.

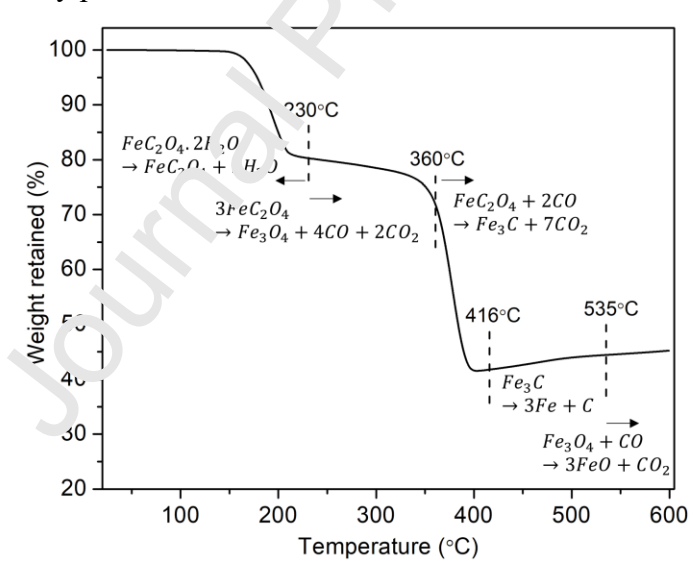


Fig. 5. Thermogravimetric analysis of ferrous oxalate precipitate.

Furthermore, Mössbauer spectroscopy was carried out to determine the quantitative fraction of different Fe phases. The Mössbauer spectra shown in Fig. 6 (b) correspond to different heating conditions, and the stick diagrams show the various phases found in the fitting. The assignment of Fe<sub>3</sub>O<sub>4</sub> is based on the isomer shift value. Quantitative analysis (statistical uncertainties of  $\pm$ 

1%) of different phases from Mössbauer data shows that the sample heated at 400 °C shows the presence of maghemite (87 %) as a major phase along with magnetite (13 %). The poor crystallization at low temperature and fine particle size resulted in the formation of maghemite. The sample heated at 450 °C for 1 h consists of 92 % magnetite and 8 % cementite. The cementite content was reduced to about 2 % after heating at 500 °C for 1 h, while magnetite content went up to 98 %.

Vibratory sample magnetometry (VSM) analysis (Fig. 6 (c)) was performed to measure the magnetic properties of the magnetite powder obtained at 500 °C, 1 h decomposition condition. The saturation magnetization of magnetite powder was determined as 80.8 emu/g, while the coercivity was 177 Oe. The high magnetic saturation value shows that the product is highly magnetic and qualifies as a high-grade magnetite product. Furthermore, the average particle size of the magnetite powder was about 16.04 microns determined using laser diffraction particle analyzer.

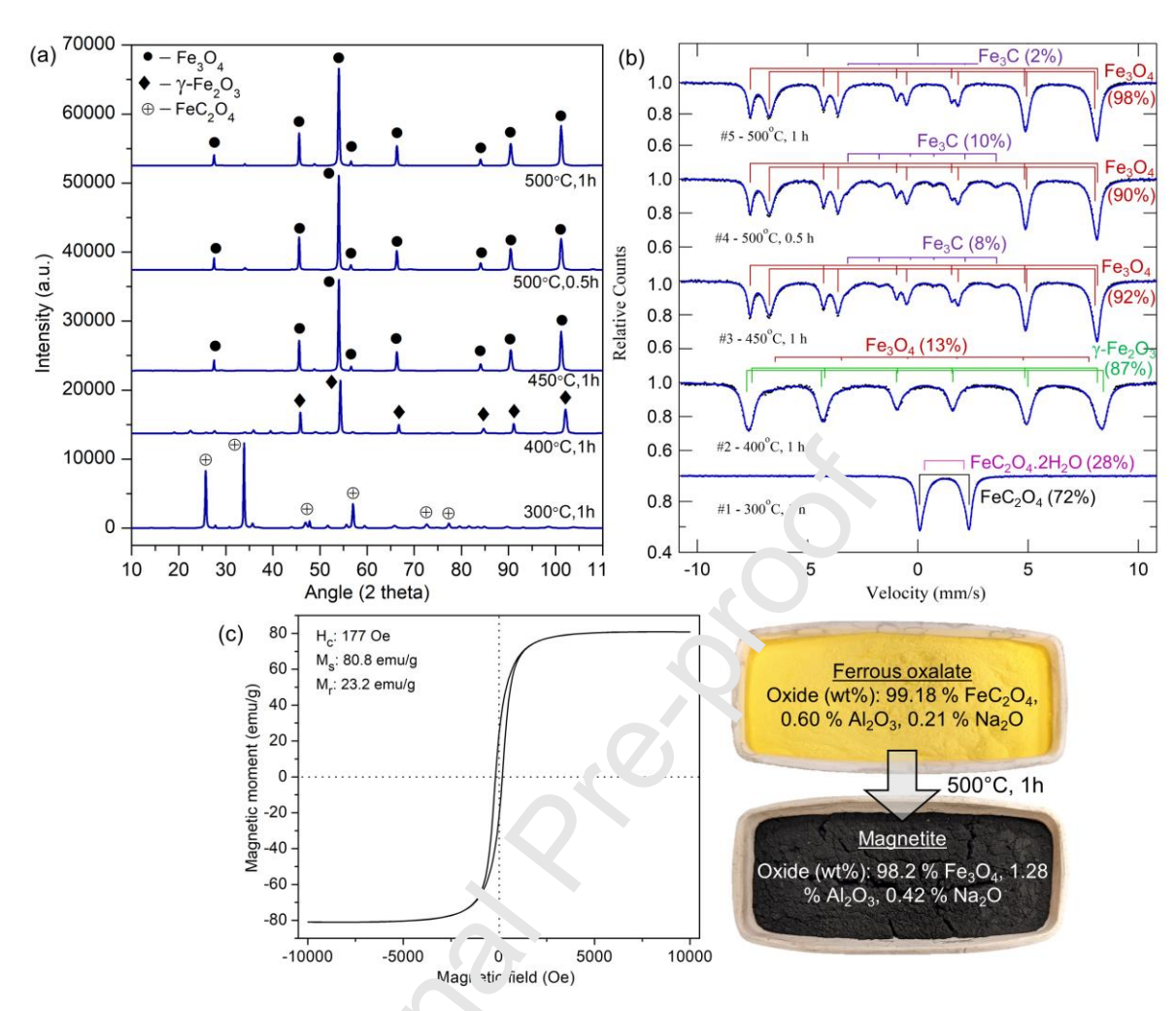


Fig. 6. Characterization of the mol decomposition of ferrous oxalate to magnetite at different temperatures: (a) XRD sportia, (b) Mössbauer spectra, (c) VSM analysis and chemical composition of magnetite at 500 °C, 1 h condition.

#### 3.4. Sulfation baking and mydrolysis for titania recovery

The sulfuric acid leaching process is commercially adopted to process ilmenite ore for Ti recovery. The method includes digestion of ilmenite in 16.7 – 18.4 M sulfuric acid solution, iron crystallization, reduction and Ti hydrolysis to recover hydrated TiO<sub>2</sub> (Han et al., 1987; Liang et al., 2005). The typical processing temperature is in the range of 100 – 200 °C using 13 – 14 M sulfuric acid. The process is successful in the dissociation and dissolution of ilmenite (FeTiO<sub>3</sub>) phase; however, TiO<sub>2</sub> phases, including rutile and anatase, behave inert (Dubenko et al., 2020). There are a few studies related to the roasting of high Ti slag with sulfuric acid at high temperature (200 – 500 °C) for Ti dissolution from TiO<sub>2</sub> phase (Sui and Zhai, 2014; Sui et al.,

2015). The studies state that the mass transfer between solid and sulfuric acid increases with an increase in temperature, thereby accelerating the reaction kinetics. The inert nature of TiO<sub>2</sub> phase during sulfuric acid leaching is due to the underlying crystal structure consisting of TiO<sub>6</sub> octahedra, in which each Ti ion is in coordination with six oxygen ions located in the octahedral system. The crystal structure consists of a densely packed oxygen ion plane parallel to the quadruple axis of rutile crystal like a spinel structure and is rigid (Dubenko et al., 2020). The breakage of -Ti-O-Ti- bond induces deformation in the crystal lattice due to the difference in ionic radii of SO<sub>4</sub><sup>2-</sup> (0.258 nm) and O<sup>2-</sup> (0.163nm). The large positive charge of Ti(IV) and its relatively large radii than other metal ions (such as Fe, Al) increase, the activation energy of the substitution reaction of oxygen ions with other ligands (SO<sub>4</sub><sup>2-</sup>). Therefore, high temperature is required to meet the additional energy requirement for TiO<sub>2</sub> phase dissociation.

Sulfation baking is a function of the decomposition behavior of sulfuric acid at high temperatures and its reactivity. Sulfuric acid decomposes to H<sub>2</sub>O and SO<sub>3</sub> predominantly in the temperature range of 127 – 427 °C. Some amount of gaseour sulfation acid is also obtained. The second stage of decomposition involves endothermic refluction of SO<sub>3</sub> to SO<sub>2</sub> and is observed at a temperature of more than 750 °C (Schwartz et al., 2000). The main advantage of sulfation baking over direct leaching includes reduced acid deman<sup>2</sup>, fast reaction kinetics and a high reaction rate.

In the context of bauxite residue. In the context of bauxite residue. In the sulfation baking is mainly explored, focusing on Sc dissolution. The sulfation baking route in ones roasting (120 - 200 °C, 2 - 24 h) of bauxite residue with sulfuric acid to generate metal culfates and further decomposition of sulfates (except Sc) at high temperatures (600 - 820 °C) and water leaching to dissolve Sc (Agrawal and Dhawan, 2021c; Alkan et al., 2018; Poira et al., 2016b). The main advantage of sulfation baking and decomposition is better selectivity for Sc dissolution than other metal ions such as Fe, Al, and Ti due to their decomposition at high temperatures. However, the process is not economically viable due to the very low concentration of Sc and high acid requirement due to the presence of other metal ions. Furthermore, Fe, Al, and Ti are neglected in the final residue and does not justify the complete recycling potential. In the present work, recovery of Ti and Sc was attempted after the recovery of major elements, including Fe, Al, and Si. It is worthwhile to mention that Ti and Sc were concentrated in the residue up to 4-fold after recovery of other elements. The residue after leaching with HCl and oxalic acid consists of approx. 10.3 % Si, 15.1

% Ti, 8.9 % Fe, 13.8 % Al and 0.0048 % Sc. Separation and recovery of major components before Ti and Sc recovery presents better selectivity, high reaction rate and reduced acid demand for downstream processing.

The underlying chemical reactions and standard Gibbs free energy for the reaction of different metal oxides present in bauxite residue with sulfuric acid are shown in Eq (17-21). The thermodynamic data shows that the reaction is thermodynamically favored where TiO<sub>2</sub> forms both Ti(SO<sub>4</sub>)<sub>2</sub> and TiOSO<sub>4</sub> phases, with Ti(SO<sub>4</sub>)<sub>2</sub> being more thermodynamically stable. Gibbs free energy for reaction of Sc is not presented due to the una vilability of Sc<sub>2</sub>(SO<sub>4</sub>)<sub>3</sub> in the database of FactSage 8.0/ HSC Chemistry 5.1 software. The stoichismetric calculations based on Eq (17-21) show that the required sulfuric acid dosage is 1.7 L per gram of solid residue for complete reaction. During the experiments, sulfuric acid was added at an excess of 15 % (1.3 mL sulfuric acid per gram solid), considering the decomposition and loss of sulfuric acid at high temperatures. Experimental trials were conducted in the temperature range of 150 - 400 °C for 2 h duration. The sulfated sample was further diss of an 0.5 M sulfuric acid at 65 °C for 90 min under continuous stirring. Dissolution of T<sub>1</sub> re juires a pH value less than 1 to prevent hydrolysis and precipitation of Ti as hydrated TiO2; therefore, leaching in mildly acidic conditions was preferred (Hixson and Plechner, 1937). The dissolution of different elements and weight loss during heating are shown in Fig. 7 (a). Weight loss data shows that the weight loss increased gradually up to 300 °C (total weight loss of 34.5%) and further saturated. Rapid weight loss in the lower temperature range con esponds to the loss of water of hydration of sulfuric acid, and decomposition of sulfuri: ac'd to SO<sub>3</sub> and H<sub>2</sub>O. The Ti and Sc dissolution increased with an increase in baking temperature to 250 °C, with the highest dissolution of 89.1 % Ti and 66.1 % Sc at 250 °C. Whereas dissolution of Fe and Al was in the range of 80 – 90 % at all the temperature conditions. Maximum Sc dissolution of 73.9 % was obtained at 400 °C; however, there was no significant increase compared to 250 °C condition (66.1 % dissolution). Therefore, a sulfation temperature of 250 °C was considered optimal. The XRD spectra of the sulfated sample and leach residue are shown in Fig. 7 (b). The XRD micrograph of the sulfated sample confirms Ti, Al, and Fe sulfate formed during sulfation after dissociation of rutile, anatase and boehmite phases. The metal sulfates were further dissolved during mild acid leaching, and the final residue consists mainly of the quartz phase. Chemical analysis of residue obtained at different sulfation temperatures is presented in Fig. 7 (c). The chemical analysis of residue

obtained at 250 °C shows that Si (17.4 %) is the major component, along with 3.9 % Ti, 2.5 % Fe, and 2.8 % Al which can be used as a filler material in construction. Furthermore, the leach liquor obtained after filtration was subjected to hydrolysis to recover dissolved Ti values.

$$TiO_{2} + 2H_{2}SO_{4} \rightarrow Ti(SO_{4})_{2} + 2H_{2}O \ (\Delta G_{25^{\circ}C}^{\circ} = -211.30 \ kJ/mol) \ (17)$$

$$TiO_{2} + H_{2}SO_{4} \rightarrow TiOSO_{4} + H_{2}O \ (\Delta G_{25^{\circ}C}^{\circ} = -163.40 \ kJ/mol) \ (18)$$

$$Sc_{2}O_{3} + 3H_{2}SO_{4} \rightarrow Sc_{2}(SO_{4})_{3} + 3H_{2}O \ (19)$$

$$Fe_{2}O_{3} + 3H_{2}SO_{4} \rightarrow Fe_{2}(SO_{4})_{3} + 3H_{2}O \ (\Delta G_{25^{\circ}C}^{\circ} = -160.49 \ kJ/mol) \ (20)$$

$$Al_{2}O_{3} + 3H_{2}SO_{4} \rightarrow Al_{2}(SO_{4})_{3} + 3H_{2}O \ (\Delta G_{25^{\circ}C}^{\circ} = -150.00 \ kJ/mol) \ (21)$$

Hydrolysis of titanium sulfate solution for TiO<sub>2</sub> recovery is w delv employed in the industrial processing of ilmenite ore (Grzmil et al., 2008; Hixson and Ple hner, 1933). The typical leach liquor obtained after sulfuric acid leaching of ilmenite and colling crystallization of excess Fe under vacuum consist of Fe to Ti mass ratio of 0.7 (71 eng et al., 2015). The leach liquor obtained after sulfation baking and leaching at optimized conditions comprised of 12311.01 ppm Ti, 7189.18 ppm Fe, and 7210.11 ppm A<sup>1</sup> Tre low Fe/Ti ratio of 0.57 in the leach liquor eliminates the Fe crystallization requirement and can be directly processed to recover Ti. As per the Pourbaix diagram, Fe in its ferrous evidation state (Fe<sup>2+</sup>) is soluble in a broad pH range from highly acidic to a mild alkaline solu ica, whereas ferric ion (Fe<sup>3+</sup>) is soluble only in the acidic range with oxidizing conditions (Eh > 0.7 V) (Monhemius, 2017). Outside these boundary conditions, Fe is insoluble and precipitates as Fe(OH)<sub>3</sub> and Fe(OH)<sub>2</sub> in acidic and alkaline conditions, respectively. To selectively recover Ti from sulfate leach solution, Fe(III) was first reduced to Fe(II) using Fe filings to prevent coprecipitation with Ti. The hydrolysis experiments without Fe reduction caused Fe precipitation and contaminated the TiO<sub>2</sub> product; therefore, reduction of Fe(III) was necessary. The XRD spectra and chemical composition of hydrated TiO<sub>2</sub> precipitate shown in Fig. 7 (d) depict the effective separation of Ti from the sulfated leach liquor and recovery of pure TiO<sub>2</sub> product. The total recovery of Ti from leach liquor was more than 96 %, with the final solution consisting of 55.10 ppm Ti, 9080.00 ppm Fe, 7190.20 ppm Al and 4.1 ppm Sc.

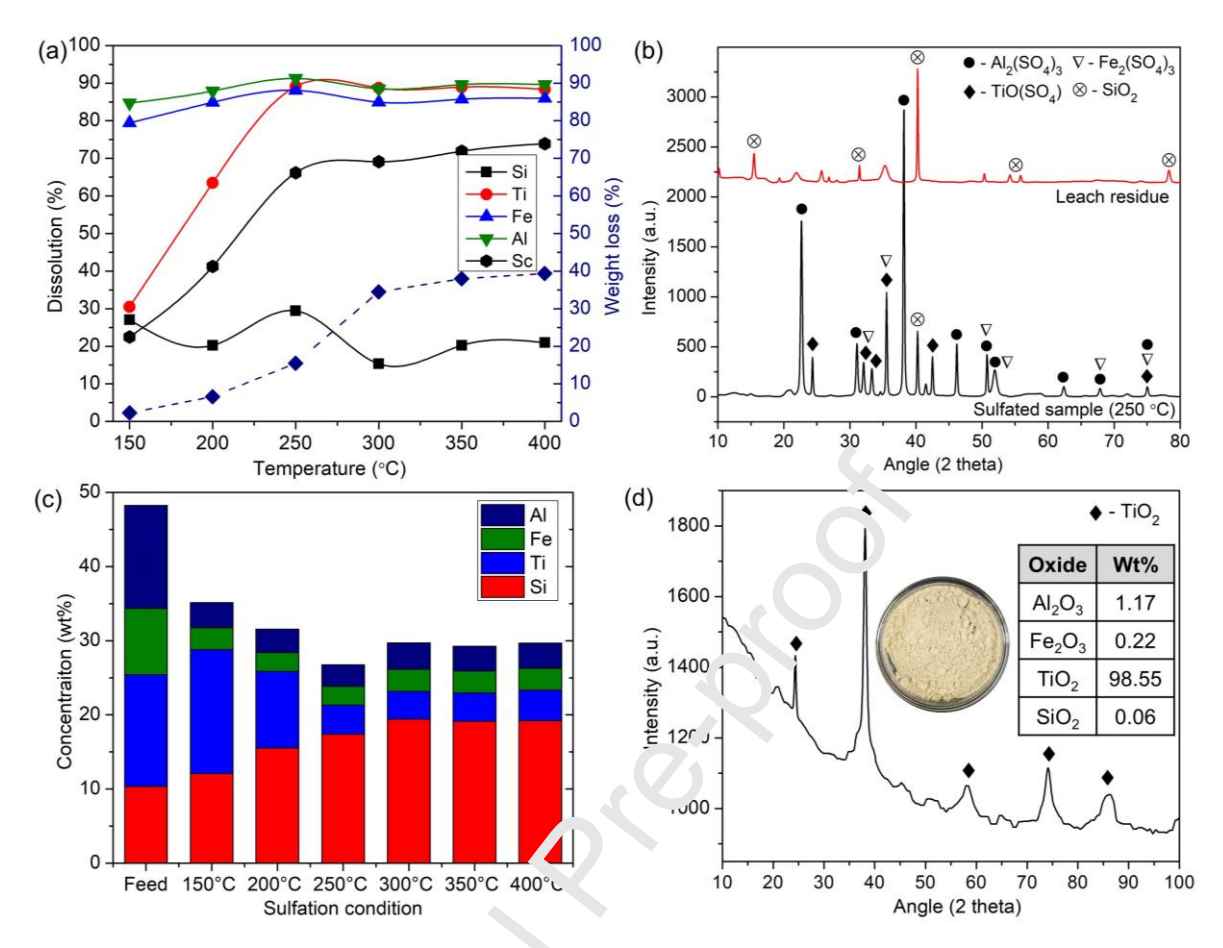


Fig. 7. (a) Dissolution (%) of different elements during sulfation-leaching at different baking temperatures, (b) XRD spectra of selfated sample and leach residue, (c) Chemical composition of residue at different temperatures, (d) XRD spectrum and chemical analysis of titania product.

#### 

Bauxite residue consists of multiple critical elements such as Sc, Ga and V with a concentration equivalent to mineral ores and can be considered a potential feedstock. Direct recovery of these elements is technically feasible but not favored economically due to low concentration (0.001 – 0.012 % RE, 0.001 – 0.011 % Ga, 0.03 – 0.23 % V) (Borra et al., 2016a; Li et al., 2021). Therefore, the concentration needs to be upgraded prior to recovering these elements. Furthermore, subsequent recovery of base metals (Fe, Ti) and critical elements (V, Sc) from bauxite residue will bolster the process economics and provide a comprehensive utilization opportunity. The behavior of Sc and V at different treatment and potential recovery stages in the proposed flowsheet is shown in Fig. 8.

The concentration of V was upgraded from 0.1074 % to 0.1534 % with only 2.5 % V dissolving during HCl leaching. Furthermore, 77.9 % of V was leached along with Fe during leaching with oxalic acid. The photochemical reduction of oxalate leach liquor separated Fe as ferrous oxalate while V remained dissolved in the solution. The solution obtained after precipitation consists of about 173.4 ppm V along with 108.1 ppm Si, 1266.1 ppm Fe, and 15113.2 ppm Al. Based on the literature, solvent extraction using Cyanex 923, and Aliquat 336 is successful in selective recovery of V from acid leach solution containing Al as major impurities (Liu et al., 2020; Wang et al., 2009).

The Sc values were upgraded from 0.0016 % to 0.0048 % in the residue obtained after leaching with oxalic acid. Approx. 66.2 % of Sc was dissolved during solution and reported to the final solution after Ti recovery. The concentration of Sc in the final solution was approx. 4.1 ppm and is consistent with the concentration of red mud leache e for Sc recovery processes in literature (Ochsenkühn-Petropoulou et al., 2002). Solvent extraction with the ionic liquid betainium bis(trifluoromethylsulfonyl)imide and adsorption on functionalized chitosan–silica hybrid materials are reported in the literature for recovery of Sc from similar leach liquors of bauxite residue (Onghena et al., 2017; Roosen et al., 2016).

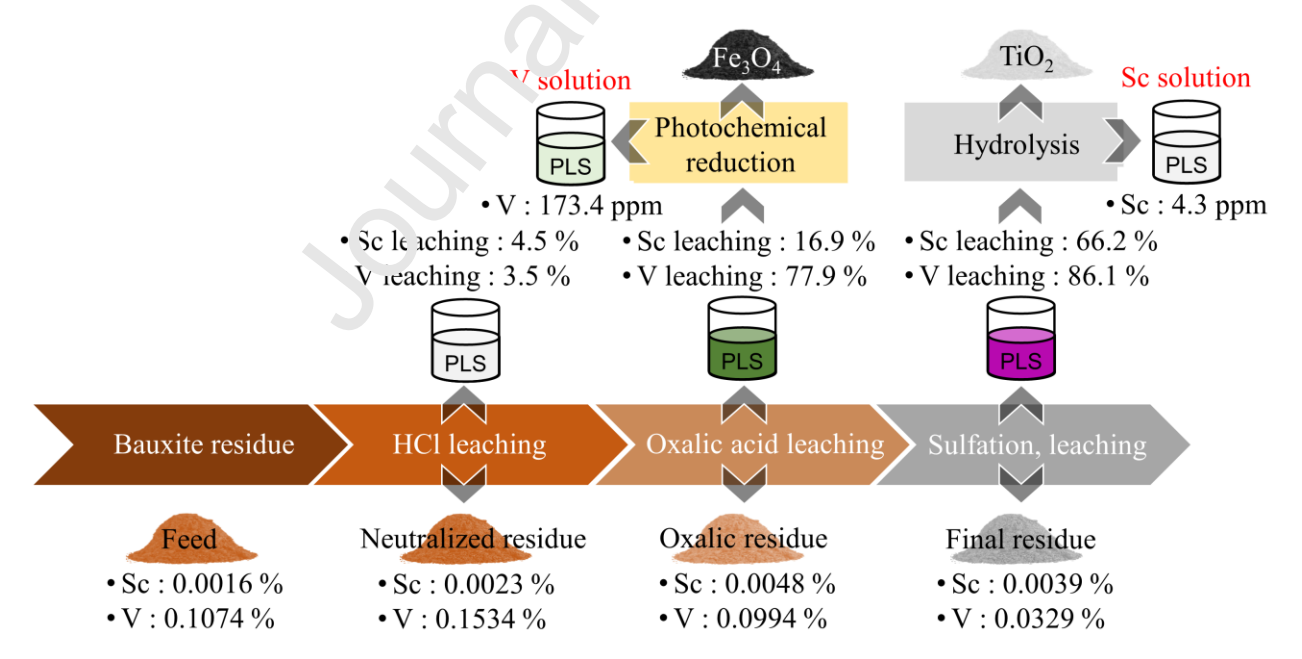


Fig. 8. Concentration and dissolution value of Sc and V at different stages of treatment.

#### 3.6. Overall flowsheet and economic analysis

A complete flowsheet (Fig. 9) for comprehensive recycling of bauxite residue is proposed based on the research work carried out. The chemical composition of the key products presented in Fig. 9 is shown in Table 2. The major elements (Fe, Al, Ti, Si, Ca) associated in bauxite residue are recovered as high purity magnetite, alumina, titania, silica and calcium carbonate. Based on the material balance, it was found that processing one ton of bauxite residue through the proposed flowsheet will result in the recovery of 254 kg magnetite, 53 kg alumina, 62 kg titanium dioxide, 110 kg silica, and 23 kg calcium carbonate. While critical elements including Sc and V are recovered into the solution containing approx. 173.39 ppm V and 4.1 ppm Sc yielding 1200.0 g V<sub>2</sub>O<sub>5</sub> and 10.9 g Sc<sub>2</sub>O<sub>3</sub>, respectively, after final recovery those gh solvent extraction/ ion exchange.

A preliminary reagent cost analysis was carried out to cases the economic feasibility of the process. The cost of chemical reagents and marketcale products was obtained from online sources such as Alibaba.com. The cost of HCl (37 %), exalic acid (99 %), H<sub>2</sub>SO<sub>4</sub> (98 %), NH<sub>4</sub>OH (35 %) and Fe powder (98 %) was considered as \$130.0-160.0/ton, \$400-450/ton, \$80-120/ton, \$150-200/ton, and \$350-400/ton espectively. Whereas, the cost of magnetite, alumina, calcium carbonate, silica, titanium d'oxide, vanadium pentoxide, and scandium oxide were considered as \$3000-5000/ton, \$1000-3000/ton, \$150-250/ton, \$10-15/ton, \$2000-5000/ton, \$40000-80000/ton, and \$550000-70000 ton respectively. As per the cost analysis, it was found that approx. +\$252.71 to +\$96. 92 profit margin is made per ton of bauxite residue processed through the proposed process. However, it is important to mention that this does not consider the capital and operating express s. Detailed life cycle assessment analysis is required to assess the economic feasibility of he process. Based on preliminary cost assessment the ranking of different marketable products with high profit margin is magnetite > titanium dioxide > alumina > vanadium pentoxide > scandium dioxide > calcium carbonate > silica. Sc and V oxide are the most critical raw materials within bauxite residue; however, the low concentration of these elements yields less product at the expense of expensive reagents; therefore, recovery of these elements as a byproduct of the base metal recovery process will favor the process economics.

A pictorial representation of the quantity of reagents required and different products generated per ton of bauxite residue is shown in Fig. 10. High purity magnetite possesses application in magnetic resonance imaging, targeted drug delivery systems, photo magnetics, and black

pigment material. Titania is mainly used as white pigment and photocatalyst. Titania can be further processed to produce Ti metal with a wide range of applications in alloys used in the engine, rotor, hydraulic system, compressor blades and nacelle. Alumina is widely utilized in manufacturing high-quality ceramics and can be electrolytically reduced to produce Al metal. Sc is mainly used in Sc-Al alloy for the aerospace industry and is considered a critical raw material for advanced manufacturing. V is used in flow batteries, catalysts, tool steel, and alloys for nuclear reactors.

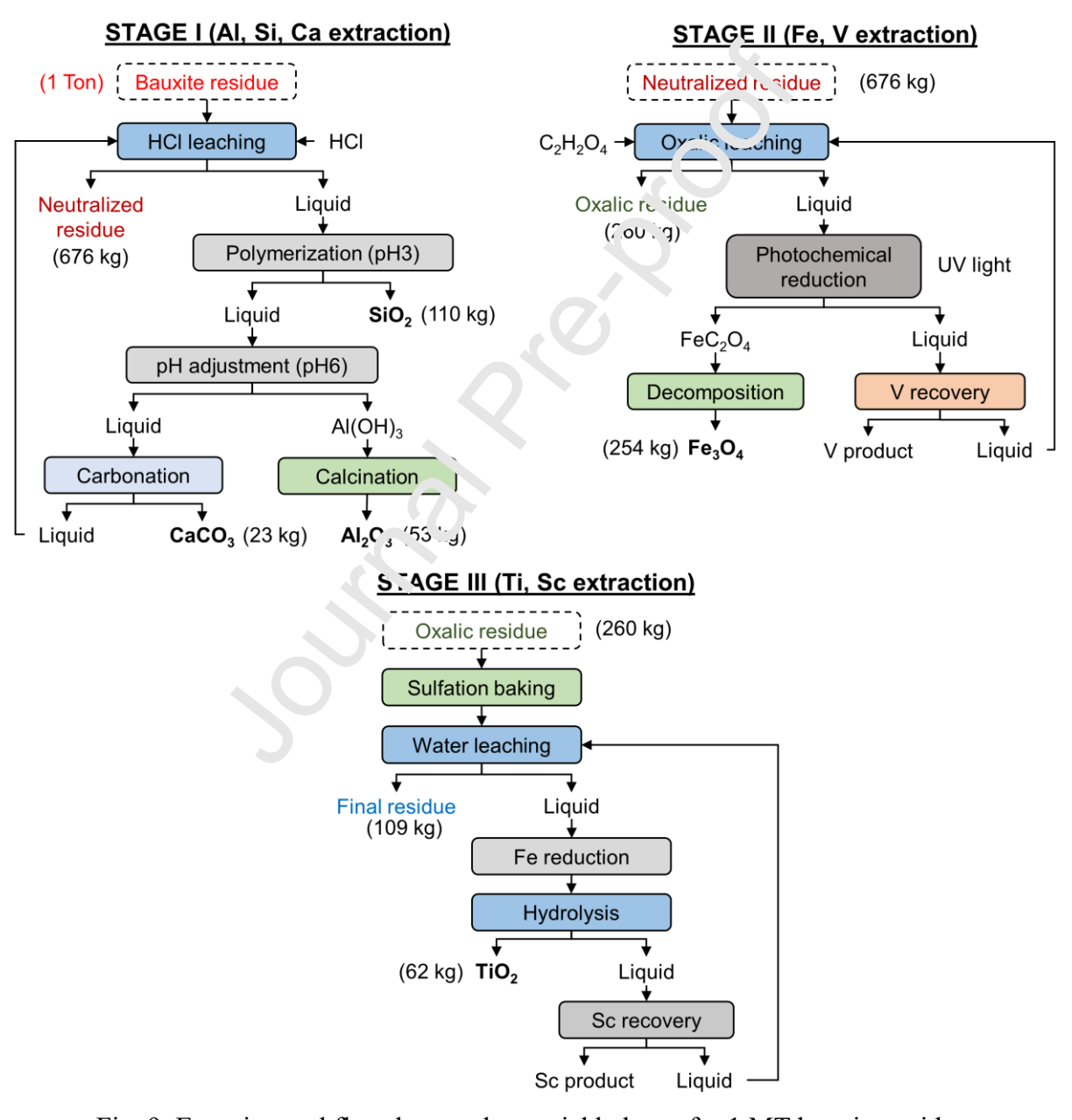


Fig. 9. Experimental flowsheet and material balance for 1 MT bauxite residue.

Table 2. Chemical of	composition of dif	fferent samples i	presented in t	he flowsheet.
Tuote 2. Chemineur	zomposition of an	iteretti battipies	presented in t	are the warren.

Sample	Quantity	Elt	CaO	SiO <sub>2</sub>	TiO <sub>2</sub>	Na <sub>2</sub> O	Fe <sub>2</sub> O <sub>3</sub>	$Al_2O_3$	$\mathbf{V}^{\mathrm{X}}$	$\mathbf{Sc}^{\mathbf{X}}$
SiO <sub>2</sub>	110 kg	%	6.13*	49.67	ı	16.70*	ı	27.50 <sup>+</sup>	-	-
$Al_2O_3$	53 kg	%	0.21	0.79	ı	0.55	ı	98.45	-	-
CaCO <sub>3</sub>	23kg	%	98.01	ı	ı	1.99	ı	ı	-	-
Fe <sub>3</sub> O <sub>4</sub>	254 kg	%	0.01	ı	ı	0.42	98.22	1.28	-	_
TiO <sub>2</sub>	62 kg	%	ı	0.06	98.55	ı	0.22	1.17	_	_
Residue	109 kg	%	0.01	70.53	12.29	0.01	6.86	10.32	0.0329	0.0039
HCl waste	7692 L	ppm <sup>#</sup>	51.00*	1.23	ı	8510.11*	ı	7.92*	-	-
V solution	6760 L	ppm <sup>#</sup>	659.00	108.11	1579.42	332.55	1266.12	15113.21	173.39	0.11
Sc							()		-	4.1
solution	2600 L	ppm <sup>#</sup>	-	-	55.10	-	9627.00	7190.20		
*(chloride), *(hydroxide), *(ion in solution), *(Carbonate)										

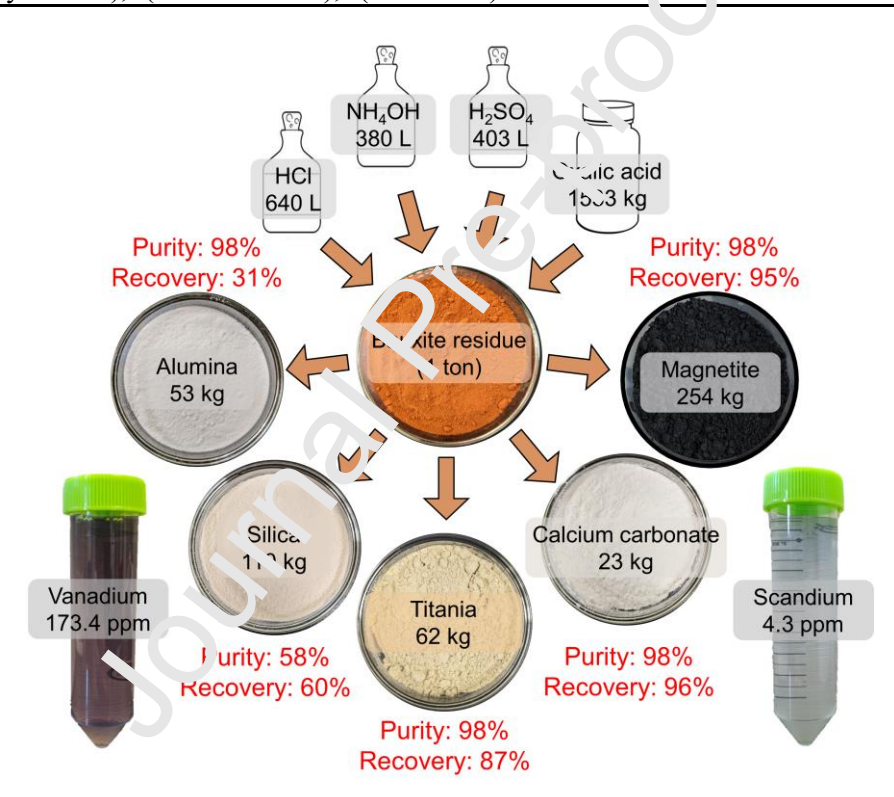


Fig. 10. Sample photographs of products generated and required reagents for the proposed process.

#### **Conclusions**

Based on the results presented in this study, the hydrometallurgy-based processing flowsheet was found superior to other processing options in terms of purity and yield of different products. The research findings indicate that the major fraction of bauxite residue (Fe, Ti, Al, Si, Ca) can be

recovered along with critical elements (V, Sc) through the proposed hydrometallurgical process flowsheet. The processing requires hydrochloric acid, sulfuric acid, oxalic acid, and ammonium hydroxide as chemical additives and are widely available on industrial scale. Furthermore, it results in the recovery of major elements of bauxite residue in the form of magnetite (98 % purity, 95 % recovery), alumina (98 % purity, 31 % recovery), titania (98 % purity, 87 % recovery), silica (58 % purity 60 % recovery), and calcium carbonate (98 % purity, 96 % recovery). Furthermore, a liquid stream of dissolved V and Sc is generated to recover critical elements. The proposed flowsheet is sustainable in recycling waste solution in the process, which results in regeneration of leaching reagent and drastically reduces acid demand and waste volume. Preliminary cost analysis shows a positive outlook with value generation of +\$252.71 to +\$969.92 per ton of bauxite residue and contributes to process development for comprehensive utilization of bauxite residue on an industrial scale.

Acknowledgment: The authors are thankful to Mr Taylor Trottier for his support in a part of the experimental work reported. The authors also wish a chank Mr. Glenn Yee, for the fellowship he instituted at the Worcester Polytechnic Inviture. Thanks are due to the NSF Center for Resource Recovery & Recovery & Recovery & LLC.

#### References

- Agrawal, S. and Dhawan, N., 2021 Eva'uation of red mud as a polymetallic source A review. Minerals Engineering, 171.
- Agrawal, S. and Dhawan, N., 2021b. Investigation of mechanical and thermal activation on metal extraction from rec must. Sustainable Materials and Technologies, 27.
- Agrawal, S. and Dhawan, N., 2021c. Microwave acid baking of red mud for extraction of titanium and scandium values. Hy drometallurgy, 204.
- Akcil, A., Akhmadiyeva, N., Abdulvaliyev, R., Abhilash and Meshram, P., 2017. Overview On Extraction and Separation of Rare Earth Elements from Red Mud: Focus on Scandium. Mineral Processing and Extractive Metallurgy Review, 39(3): 145-151.
- Alkan, G. et al., 2018. Novel Approach for Enhanced Scandium and Titanium Leaching Efficiency from Bauxite Residue with Suppressed Silica Gel Formation. Sci Rep, 8(1): 5676.
- Anawati, J. and Azimi, G., 2019. Recovery of scandium from Canadian bauxite residue utilizing acid baking followed by water leaching. Waste Manag, 95: 549-559.
- Anawati, J. and Azimi, G., 2020. Recovery of Strategic Materials from Canadian Bauxite Residue by Smelting Followed by Acid Baking–Water Leaching. Rare Metal Technology 2020. Springer International Publishing, Cham, pp. 139-150.
- Archambo, M. and Kawatra, S.K., 2020a. Red Mud: Fundamentals and New Avenues for Utilization. Mineral Processing and Extractive Metallurgy Review, 42(7): 427-450.

- Archambo, M.S. and Kawatra, S.K., 2020b. Utilization of Bauxite Residue: Recovering Iron Values Using the Iron Nugget Process. Mineral Processing and Extractive Metallurgy Review, 42(4): 222-230.
- Balomenos, E., Gianopoulou, I., Panias, D. and Paspaliaris, I., 2012. A novel red mud treatment process. CRETE 2012.
- Balomnenos, E., Kastritis, D., Panias, D., Paspaliaris, I. and Boufounos, D., 2016. The Enexal Bauxite Residue Treatment Process: Industrial Scale Pilot Plant Results. In: J. Grandfield (Ed.), Light Metals 2014. Springer International Publishing, Cham, pp. 143-147.
- Borra, C.R., Blanpain, B., Pontikes, Y., Binnemans, K. and Van Gerven, T., 2015a. Smelting of Bauxite Residue (Red Mud) in View of Iron and Selective Rare Earths Recovery. Journal of Sustainable Metallurgy, 2(1): 28-37.
- Borra, C.R., Blanpain, B., Pontikes, Y., Binnemans, K. and Van Gerven, T., 2016a. Recovery of Rare Earths and Other Valuable Metals From Bauxite Residue (Red Mud): A Review. Journal of Sustainable Metallurgy, 2(4): 365-386.
- Borra, C.R. et al., 2016b. Selective recovery of rare earths from bounite residue by combination of sulfation, roasting and leaching. Minerals Engineering, 92: 15.-15%.
- Borra, C.R., Pontikes, Y., Binnemans, K. and Van Gerven, T., 2015'. Le ching of rare earths from bauxite residue (red mud). Minerals Engineering, 76: 20-27.
- Bray, E.L., 2021. Aluminum. U.S. Geological Survey, Mineral Campinadity Summaries.
- Cardenia, C., Balomenos, E. and Panias, D., 2018. Iron Recovery from Bauxite Residue Through Reductive Roasting and Wet Magnetic Separation. Journal of Custainable Metallurgy, 5(1): 9-19.
- Di Carlo, E., Boullemant, A. and Courtney, R., 2020 F.ctoxicological risk assessment of revegetated bauxite residue: Implications for future rehabilitation programmes. Sci Total Environ, 698: 134344.
- Dietzel, M., 2000. Dissolution of silicates and the stability of polysilicic acid. Geochimica et Cosmochimica Acta, 64(19): 3275-3281.
- Dimas, D., Giannopoulou, I. and Panias 2. 2009. Polymerization in sodium silicate solutions: a fundamental process in geopo'yr e ization technology. Journal of Materials Science, 44(14): 3719-3730.
- Ding, W., Bao, S., Zhang, Y. and Xizo, 1, 2022. Efficient Selective Extraction of Scandium from Red Mud. Mineral Processing and Fxt. active Metallurgy Review: 1-9.
- Dubenko, A.V., Nikolenko, M.V., Nesenenko, E.V., Kostyniuk, A. and Likozar, B., 2020. Mechanism, Thermodynamics and Vinctics of Rutile Leaching Process by Sulfuric Acid Reactions. Processes, 8(6).
- Evans, K., 2016. The History Challenges, and New Developments in the Management and Use of Bauxite Residue. Journal of Justainable Metallurgy, 2(4): 316-331.
- Giannopoulou, I. and Panias, D., 2010. Hydrolytic stability of sodium silicate gels in the presence of aluminum. Journal of Materials Science, 45(19): 5370-5377.
- Grzmil, B.U., Grela, D. and Kic, B., 2008. Hydrolysis of titanium sulphate compounds. Chemical Papers, 62(1): 18-25.
- Habashi, F., 2005. A short history of hydrometallurgy. Hydrometallurgy, 79(1-2): 15-22.
- Habashi, F., 2016. A Hundred Years of the Bayer Process for Alumina Production, Essential Readings in Light Metals, pp. 85-93.
- Han, K.N., Rubcumintara, T. and Fuerstenau, M.C., 1987. Leaching behavior of ilmenite with sulfuric acid. Metallurgical Transactions B, 18(2): 325-330.
- Healy, S., 2022. Sustainable Bauxite Residue Management Guidance, International Aluminum Institute.
- Hench, L.L. and West, J.K., 1990. The Sol-Gel Process. Chem. Rev., 90: 33-72.

- Hermanek, M., Zboril, R., Mashlan, M., Machala, L. and Schneeweiss, O., 2006. Thermal behaviour of iron(ii) oxalate dihydrate in the atmosphere of its conversion gases. Journal of Materials Chemistry, 16(13).
- Hixson, A.W. and Plechner, W.W., 1933. Hydrated Titanium Oxide. Thermal Precipitation from Titanium Sulfate Solutions. Industrial & Engineering Chemistry, 25(3): 262-274.
- Hu, P. and Zhang, Y., 2021. Mechanism of vanadium selective separation from iron in shale under an environmentally friendly oxalate ligand system. Separation and Purification Technology, 276.
- Khairul, M.A., Zanganeh, J. and Moghtaderi, B., 2019. The composition, recycling and utilisation of Bayer red mud. Resources, Conservation and Recycling, 141: 483-498.
- Lee, S.O., Tran, T., Park, Y.Y., Kim, S.J. and Kim, M.J., 2006. Study on the kinetics of iron oxide leaching by oxalic acid. International Journal of Mineral Processing, 80(2-4): 144-152.
- Li, W., Yan, X., Niu, Z. and Zhu, X., 2021. Selective recovery of vanadium from red mud by leaching with using oxalic acid and sodium sulfite. Journal of Environmental Cramical Engineering, 9(4).
- Liang, B., Li, C., Zhang, C. and Zhang, Y., 2005. Leaching kinetics of Panchinua ilmenite in sulfuric acid. Hydrometallurgy, 76(3-4): 173-179.
- Liu, Z. et al., 2020. Separation and recovery of vanadium and aum num from oxalic acid leachate of shale by solvent extraction with Aliquat 336. Separation and Curification Technology, 249.
- Majima, H., Awakura, Y. and Mishima, T., 1985. The leaching of nomatite in acid solutions. Metallurgical Transactions B, 16B: 23-30.
- Mangiante, D.M., Schaller, R.D., Zarzycki, P., Banfield, J.F. and Gilbert, B., 2017. Mechanism of Ferric Oxalate Photolysis. ACS Earth and Space Chem 1st. y 1(5): 270-276.
- Marin Rivera, R. and Van Gerven, T., 2020. Product on of calcium carbonate with different morphology by simultaneous CO2 capture and minoral sation. Journal of CO2 Utilization, 41.
- Mishra, B. and Gostu, S., 2017. Materials suscir ability for environment: Red-mud treatment. Frontiers of Chemical Science and Engineering, 11(s): 483-496.
- Mishra, B., Staley, A. and Kirkpatrick, D., 2002 Recovery of value-added products from red mud. Mining Metallurgy and Exploration, 19: 37 9.
- Monhemius, J., 2017. The iron elephant: ∴ brief history of hydrometallurgists' struggles with element no. 26. CIM Journal, 8: 197 2.5.
- Ochsenkühn-Petropoulou, M.T., Hetzilyberis, K.S., Mendrinos, L.N. and Salmas, C.E., 2002. Pilot-Plant Investigation of the Leaching Process for the Recovery of Scandium from Red Mud. Industrial & Engineering Chemist., Research, 41(23): 5794-5801.
- Onghena, B., Borra, C.R. Van Gerven, T. and Binnemans, K., 2017. Recovery of scandium from sulfation-roasted leachates of bauxite residue by solvent extraction with the ionic liquid betainium bis(trifluoromethy/Sulfonyl)imide. Separation and Purification Technology, 176: 208-219.
- Reid, S., Tam, J., Yang, M. and Azimi, G., 2017. Technospheric Mining of Rare Earth Elements from Bauxite Residue (Red Mud): Process Optimization, Kinetic Investigation, and Microwave Pretreatment. Sci Rep, 7(1): 15252.
- Rivera, R.M., Ounoughene, G., Borra, C.R., Binnemans, K. and Van Gerven, T., 2017. Neutralisation of bauxite residue by carbon dioxide prior to acidic leaching for metal recovery. Minerals Engineering, 112: 92-102.
- Roosen, J. et al., 2016. Recovery of scandium from leachates of Greek bauxite residue by adsorption on functionalized chitosan–silica hybrid materials. Green Chemistry, 18(7): 2005-2013.
- Ruyters, S. et al., 2011. The red mud accident in ajka (hungary): plant toxicity and trace metal bioavailability in red mud contaminated soil. Environ Sci Technol, 45(4): 1616-22.
- Salmimies, R., Mannila, M., Kallas, J. and Häkkinen, A., 2012. Acidic dissolution of hematite: Kinetic and thermodynamic investigations with oxalic acid. International Journal of Mineral Processing, 110-111: 121-125.

- Schwartz, D., Gadiou, R., Brilhac, J.-F., Prado, G. and Martinez, G., 2000. A Kinetic Study of the Decomposition of Spent Sulfuric Acids at High Temperature. Industrial & Engineering Chemistry Research, 39(7): 2183-2189.
- Sui, L.-l. and Zhai, Y.-c., 2014. Reaction kinetics of roasting high-titanium slag with concentrated sulfuric acid. Transactions of Nonferrous Metals Society of China, 24(3): 848-853.
- Sui, L.-L., Zhai, Y.-C. and Miao, L.-H., 2015. Recovery of titania from high titanium slag by roasting method using concentrated sulfuric acid. Rare Metals, 34(12): 895-900.
- Swain, B., Akcil, A. and Lee, J.-c., 2020. Red mud valorization an industrial waste circular economy challenge; review over processes and their chemistry. Critical Reviews in Environmental Science and Technology: 1-51.
- Tanvar, H. and Mishra, B., 2021. Hydrometallurgical Recycling of Red Mud to Produce Materials for Industrial Applications: Alkali Separation, Iron Leaching and Extraction. Metallurgical and Materials Transactions B, 52: 3543–3557
- Taxiarchou, M., Panias, D., Douni, I., Paspaliaris, I. and Kontopoulos, 1., 1957. Dissolution of hematite in acidic oxalate solutions. Hydrometallurgy, 44(3): 287-299.
- Tsakiridis, P.E., Agatzini-Leonardou, S. and Oustadakis, P., 2004. Red mud addition in the raw meal for the production of Portland cement clinker. J Hazard Ma er, 11o(1-2): 103-10.
- Ujaczki, É. et al., 2019. Recovery of Gallium from Bauxite Residue Using Combined Oxalic Acid Leaching with Adsorption onto Zeolite HY. Journal of Sustainable Metallurgy, 5(2): 262-274.
- Ujaczki, E. et al., 2018. Re-using bauxite residues: benefi.s beyond (critical raw) material recovery. J Chem Technol Biotechnol, 93(9): 2498-2510.
- Wang, M., Zhang, G., Wang, X. and Zhang, J., 200°. Solicent extraction of vanadium from sulfuric acid solution. Rare Metals, 28(3): 209-211.
- Zheng, L., Liang, B., Lü, L., Jia, L. and Li, C 2015. Effect of impurities on the hydrolysis of low-concentration titanyl sulfate solutions. Research on Chemical Intermediates, 41(8): 5423-5438.

## CRediT author statement

**Himanshu Tanvar**: Conceptualization, Investigation, Formal analysis, Writing - Original Draft; **Brajendra Mishra**: Conceptualization, Validation, Writing - Review & Editing, Supervision

#### **Declaration of interests**

that could have appeared to influence the work reported in this paper.
☐The authors declare the following financial interests/personal relationships which may be considered
as potential competing interests: